Clinical Pilot Application of Super-Resolution US Imaging in Breast Cancer

Stefanie Dencks, *Member, IEEE*, Marion Piepenbrock, Tatjana Opacic, Barbara Krauspe, Elmar Stickeler, Fabian Kiessling, and Georg Schmitz, *Senior Member, IEEE*

***Abstract*— Recently, we proved in the first measurements of breast carcinomas the feasibility of super-resolution ultrasound (US) imaging by motion-model ultrasound localization microscopy in a clinical setup. Nevertheless, pronounced in-plane and out-of-plane motions, a nonoptimized microbubble injection scheme, the lower frame rate and the larger slice thickness made the processing more complex than in preclinical investigations. Here, we compare the results of state-of-the-art contrast-enhanced to super-resolution US imaging and systematically analyze the measurements to get indications for the improvement of image acquisition and processing in the future clinical studies. In this regard, the application of a saturation model to the reconstructed vessels is shown to be a valuable tool not only to estimate the measurement times necessary to adequately reconstruct the microvasculature but also for the validation of the measurements. The parameters from this model can also serve to optimize contrast agent concentration and injection protocols. Finally, for the measurements of well-perfused tumors, we observed between 28% and 50% filling for 90-s examination times.**

***Index Terms*— Cancer, clinical imaging, localization, maximum intensity over time (MIOT), measurement times, microbubbles (MBs), motion, saturation model, super-resolution, tumors, vasculature.**

I. Introduction

WITH super-resolution ultrasound (US) imaging based on the detection and localization of microbubbles (MBs), termed as ultrasound localization microscopy (ULM), the microvasculature can be visualized below the diffraction limit of the imaging system [1], [2]. Furthermore, the emerging field of tracking the MBs over several frames provides not only impressive reconstructions of the organization of microvessels but even also functional information on blood flow velocities and directions. In this context, Christensen-Jeffries *et al.* [3] showed the blood supply in a mouse ear, Errico *et al.* [4] the perfusion of a rat brain, and Ackermann and Schmitz [5] the microvasculature in murine xenograft tumors. All these works reached resolutions beyond the resolution limits of the US devices, while applying different techniques in imaging (conventional line-by-line imaging [3], [5] or ultrafast plane-wave imaging [4]), in the detection of the MBs (in the B-mode images [3], [5] or in the RF-single-channel data [4]), and in the tracking of the MBs (using nearest neighbor tracking [3], [4] or statistical approaches [5]). They also have in common that their applications were focused on preclinical measurements that were used for proof-of-principle studies.

The clinical interest in the microvasculature of tissues is manifold because deviations from normal vessel growth play a role in numerous diseases, such as inflammatory or ulcerative disorders, cancer, or blinding eye diseases [6]. Particularly for tumors, it is known that their vascularization is morphologically abnormal [7] and that features like the tortuosity of vessels, their branching, their irregular vessel diameters, and the inhomogeneity throughout the tumor contain vital information on its aggressiveness [7], [8]. For example, the microvascular density can be used to predict tumor invasion, metastasis, and patient prognosis [9]. However, for a routine examination of tumor microvasculature the established imaging techniques lack either noninvasiveness (e.g., histology, microscopy, and micro-computed tomography), imaging depth or volume (e.g., intravital microscopy, optical coherence tomography, and optoacoustic imaging) or resolution (e.g., computed tomography and magnetic resonance tomography). Also, the state-of-the-art contrast-enhanced US (CEUS) imaging is limited by the spatial resolution of the conventional US devices. Thus, a comprehensive insight into the microvascular architecture is not possible because the voxels are usually much larger than the majority of tumor blood vessels. Therefore, also the relative blood volume (rBV) determined from the maximum intensity over time (MIOT) [10], [11] tends to be overestimated [2]. Functional parameters such as the time-to-peak, peak enhancement, and upslope of conventional time–intensity curves [10], [12] are limited to a global interpretation of perfusion. Furthermore, their assessment is difficult and unreliable at the single voxel level [13]. By revealing vascular features at super-resolution and quantifying even very low flow velocities of single vessels, ULM is expected to substantially improve the differential diagnosis, prognostication, and the monitoring and prediction of therapy responses. However, the potential of ULM is strongly interrelated with the technical feasibility in a clinical setup.

For the implementation of ULM on conventional clinical US devices, we already presented the Markov chain Monte Carlo data association (MCMCDA) algorithm to track the

Manuscript received June 28, 2018; accepted September 20, 2018. Date of publication September 24, 2018; date of current version March 14, 2019. This work was supported by the DFG under Grant SCHM1171/4-1 and Grant KI1072/11-1. *(Corresponding author: Stefanie Dencks.)*

S. Dencks, M. Piepenbrock, and G. Schmitz are with the Chair of Medical Engineering, Department of Electrical Engineering and Information Technology, Ruhr University Bochum, 44780 Bochum, Germany (e-mail: stefanie.dencks@rub.de).

T. Opacic and F. Kiessling are with the Institute for Experimental Molecular Imaging, Center for Biohybrid Medical Systems, RWTH University Clinic Aachen, 52074 Aachen, Germany (e-mail: fkiessling@ukaachen.de).

B. Krauspe and E. Stickeler are with the Department of Obstetrics and Gynecology, RWTH University Clinic Aachen, 52074 Aachen, Germany.

This paper has supplementary downloadable material at http://ieeexplore.ieee.org, provided by the authors.

Digital Object Identifier 10.1109/TUFFC.2018.2872067

MBs [5]. By accounting for the prior probabilities and a motion model, this statistical approach searches for associations of MBs which maximize the posterior probability of track associations. We also demonstrated the advantages of this algorithm in terms of estimation accuracy of tracks and velocities in complex vessel morphologies and for difficult measurement conditions [14]. To distinguish this approach from others, we termed it motion-model-based ULM (mULM). Recently, we showed that different tumor types in mice could be classified based on the structural information obtained from mULM [15].

In [15], we also presented a first proof of principle of super-resolution US imaging in a clinical setup by applying mULM to initial clinical measurements of breast cancer. Here, we systematically analyze these measurements in preparation of a larger clinical study. We report and discuss in detail the challenges we faced in the clinical setup, such as stronger motions, the increased slice thickness of the US imaging plane, highly varying MBs concentrations during one measurement, or the necessity to use the contrast mode for displaying the MBs and, thus, reducing the frame rate even further. Therefore, Section II is divided into two parts. The first part includes the general description of the clinical study design, image acquisition and processing, and the tracking of the MBs. Here, also solutions for some of the above-mentioned problems are proposed. The second part is focused on the evaluation of current limitations. Specifically, the measurement times necessary to extract reliable and meaningful parameters are investigated using an exponential saturation model. In the results, we report estimates of sufficient measurement times and compare the resulting super-resolution images of tumor vasculature to images acquired by the established MIOT method. These images exemplify the opportunities and challenges when translating ULM into clinical practice. Additional graphs are presented to visualize the difficulties due to highly varying MB concentrations and out-of-plane motion, and to outline possible strategies. Since this is not a clinical study, we will not discuss clinical findings.

II. Materials and Methods

A. Clinical Measurements

The clinical CEUS data were acquired at the Department of Gynecology and Obstetrics, University Medical Center, RWTH University, Aachen, Germany. The study is registered at clinicaltrials.gov under the number NCT03385200 and was approved by the RWTH Aachen University ethics committee. Written informed consent was obtained from all participants for CEUS imaging and the use of data for studying neoadjuvant chemotherapy responses. Here, measurement data of a triple-negative breast carcinoma in a patient treated with neoadjuvant chemotherapy were retrospectively evaluated. Measurements were performed before and after the first, second, and third cycles of chemotherapy.

For the measurements, the patient was lying supine in a stable position with the arm at the tumor side raised above the head. The CEUS measurements were performed handheld in the contrast harmonic imaging mode with a 10-MHz PLT 1005BT linear transducer (bandwidth 7–14 MHz) connected to an Aplio 500 (Canon Medical Systems, Otawara, Japan). Ten seconds after the start of the recording, a 0.5 mL of SonoVue (Bracco, Milan, Italy) were manually injected over 10 s. The mechanical index during the examinations was 0.07, and a thermal index was below 0.4. The elevational resolution at the elevational focus in 20 mm depth is 1 mm (communicated by Canon Medical Systems). Both the B-mode images and contrast mode images were recorded with a frame rate of 15 Hz. At each patient examination, two measurements each of 1350 frames (equivalent to 90 s) were carried out.

B. Image Processing

All the following procedures were implemented in MATLAB (Mathworks, Natick, MA, USA).

Although the clinical investigators were highly sensitized to minimize movement artifacts, the clinical data exhibited strong out-of-plane motion. Therefore, each measurement was subdivided into subsequences, each containing only similar image planes. This was done by a cross-correlation of the B-mode images of an interactively selected region of interest (ROI) with sufficient contrast. The cross-correlation between the two frames had to be higher than 0.8 to be assigned into one sequence. Then, each sequence was evaluated separately. To ensure a precise motion compensation, an affine image registration proposed by Rueckert *et al.* [16] (available on [17]) was applied to the B-mode images. (Always the first frame of a sequence was the reference frame.) This implementation allows translation, rotation, resizing, and shearing, and provides the transformation matrix. Because the MBs were not visible in the B-mode sequences, the motion estimation was not disturbed.

C. Detection of Microbubbles

Because the MBs were not visible in the B-mode images, they had to be detected in the contrast mode sequences. To lower the number of false detections, the contrast mode images were normalized to the maximum intensity of the sequence and all intensity values below 0.15 were set to 0. For a higher localization accuracy, the images were interpolated to a grid size of 5 μm (using the spline interpolation provided in the interp2.m function of MATLAB). Then, a 2-D convolution of the contrast mode images with a Gaussian kernel was applied. To match the point spread function of an MB in the images, the standard deviation of the Gaussian kernel was set to $\sigma = 335$ μm. By detecting the local maxima, the positions of the MBs were determined with subpixel accuracy compared to the original data. Finally, these positions were corrected by the estimated motion in the B-mode images.

D. Tracking

For the reconstruction of the microvasculature, the detected MBs were tracked over several frames. This can be achieved with a nearest neighbor tracking in case of very high frame rates (ultrafast imaging) or in case of very low MB concentrations and consequently long observation times. However, for the tracking of MBs in complex vessel morphologies and

under clinical measurement conditions, it is recommendable to use a more robust method [14]. Due to the elevational width of the imaging slice, an apparent crossing of capillaries is to be expected when capillaries of different directions are running in different planes within the slice. In addition, the low applicable frame rate, the expected flow velocities, and the highly varying MB concentrations may lead to false associations of detected positions when using a nearest neighbor tracking because the detections can be associated with tracks in different ways. Therefore, the MCMCDA algorithm [18] was applied [5] which aims to find the associations ω (assigning MBs to tracks) of detected positions Y that maximize the *a posteriori* probability $P(\omega|Y)$

$$\omega_{\max} = \arg\max_{\omega\in\Omega} P(\omega|Y). \tag{1}$$

By Bayes' rule, this *a posteriori* probability is proportional to

$$P(\omega|Y)\sim P(Y|\omega)P(\omega) \tag{2}$$

with the likelihoods $P(Y|\omega)$ of the detected positions Y under the given track associations ω. These are determined from a linear motion model realized with a Kalman filter, and with the *a priori* probabilities $P(\omega)$ of track associations, which contain, e.g., assumptions of the false alarm rate and the detection probability. Since trying all possible track combinations to find $\omega_{\max}$ is an intractable combinatorial problem, the MCMCDA randomly draws associations with the probability distribution and the best association is kept.

Although the expected velocities in capillaries are below 2.5 mm/s, the maximum velocity was set to be 7 mm/s because in this study also larger vessels with higher velocities were imaged.

E. Visualization

Several options to illustrate the microvasculature arise from the gained tracking data. Generally, it needs to be decided whether new data should be overlaid on the standard B-mode images [2] (or volume [19]), or whether it should be shown separately [3], [4]. Already established are the so-called probability density [3] or localization [4] maps, where the brightness represents the number of detections per pixel location. These are particularly applicable in case of a high number of detections. In case of short measurement times or low frame rates, these maps can be improved by not only counting the detections but also the passing of tracks through a pixel, called occurrence maps [15]. Alternatively, the detections [3] or the tracks [4], [15] can be color-coded by the determined flow velocities or directions of flow. Based on the direction information, also a coloring of the velocities comparable to Doppler mode imaging is feasible [4], [15]. Furthermore, to improve image quality (reduce noise) or to highlight different aspects, several criteria can be combined for the imaging, e.g., only showing tracks with more than three detections [4] or the combination of certain velocities and directions [15]. Here, we computed occurrence, velocity, and direction maps. For this, only tracks of more than two detections were plotted.

F. Saturation Model

The area in an image slice covered by the fully reconstructed vessel trees is expected to be proportional to the rBV. Until now, due to the limited measurement times or, rather, the limited length of evaluable sequences in the clinical application, we could not extract the complete vasculature. However, to get an estimate of the final rBV, we introduced an exponential saturation model which is based on the assumption that the reconstruction of new vessels saturates over measurement time and proved it valid in a preclinical study [20]. For this, the coverage C is defined as the ratio of the area filled with tracks to the total area of the tumor. After the coverage C has been computed as a function of the tracked MBs by charting the tracks frame by frame into a matrix of 10-μm resolution, the exponential saturation model

$$C(\mathrm{MB}(t)) = C_{\mathrm{final}}(1 - \exp(-\alpha \mathrm{MB}(t))) \tag{3}$$

with the number of tracked MB(t) until time t was fitted to the curve of C. Thus, the saturation value final coverage C_{final} is equivalent to rBV. Furthermore, the quality of fit (R^2) and the percentage of the reconstruction pR

$$pR = \frac{C(\mathrm{MB}(t_{\mathrm{meas}}))}{C_{\mathrm{final}}} \tag{4}$$

after the measurement time t_{meas} were evaluated.

To check the measurement times necessary to get a reliable estimate of rBV, also the estimated final coverage eC_{final} for shortened measurement durations was investigated. For this, the measurement durations were increased stepwise by 50 frames until reaching the final t_{meas}.

G. Conventional CEUS: MIOT

Because MIOT showed a higher robustness and accuracy than the other standard CEUS methods [10], it was used for the determination of rBV (reference method). To guarantee comparable preconditions, the images of the contrast mode were also motion corrected with the motion estimated in the B-mode images. Generally, for the generation of MIOT images, in each pixel of a sequence, the median intensity value over time is subtracted from the maximum intensity value over time

$$I_{\mathrm{MIOT}}(x,z) = \max_t(I(x,z,t)) - \mathrm{med}_t(I(x,z,t)). \tag{5}$$

This way, the background is suppressed in case of static structures. Here, the background suppression was not necessary because no static structures were existent in the contrast mode sequences. Applying an empirically determined threshold of 0.4 to the normalized MIOT data, the vessels were segmented, and the rBV was calculated as the fraction of vessel area in the tumor area.

Since the computation of MIOT suffers from the same limitations as the tracking of MBs due to the shortness of the evaluable sequences, again the exponential saturation model was applied. For this, the development of the calculated rBV over time t was computed by applying the same procedure to the measurement sequences reduced to the equivalent number

TABLE I
OVERVIEW OF MEASUREMENTS AND RESULTS FROM MIOT AND MULM

examination / measurement / sequence		**e1** / m2 / s1	**e2** / m1 / s5	**e3** / m2 / s1	**e4** / m1 / s1	**e4** / m2 / s1
	number of frames	764	705	1349	1049	1349
	motion in µm	277 ± 165	574 ± 339	222 ± 109	405 ± 179	475 ± 412
	number of tracked MB	150	21483	8163	1061	2038
MIOT	rBV(t_{meas}) in %	0.23	81.49	53.25	18.09	30.55
	rBV$_{\text{final}}$ in %	**0.35**	**78.6**	**55.7**	**21.2**	**39.2**
	pR in %	65.9	103.7	95.6	85.1	77.8
	R^2	0.977	0.97	0.99	0.98	0.98
mULM	$C(t_{\text{meas}})$ in %	0.02	8.48	3.27	0.84	1.43
	C_{final} in %	**0.06**	**18.8**	**6.6**	**31.1**	**120.6**
	pR in %	28.5	45.2	49.9	2.7	1.2
	R^2	0.98	0.9997	0.9988	0.955	0.976

rBV: relative blood volume, pR: percentage of reconstruction, R^2: quality of fit, C: coverage.

of frames. This would generally be

$$I_{\text{MIOT}}(x, z, t_{\text{frame}}) = \max_t(I(x, z, t \le t_{\text{frame}})) - \operatorname{med}_t(I(x, z, t \le t_{\text{frame}})) \quad (6)$$

but again, the background subtraction could be disregarded.

Then, the equivalent saturation model

$$\text{rBV(t)} = \text{rBV}_{\text{final}}(1 - \exp(-\alpha t)) \quad (7)$$

was fitted to the derived rBV values.

In the case of low MB concentrations at the beginning of a measurement sequence, the section selected for the exponential fit was chosen interactively. Just as for the mULM data, also the estimated final erBV$_{\text{final}}$ for shortened measurement durations was investigated (see Section II-F).

III. RESULTS

From the eight measurements (two per examination), the first measurement of the third examination could not be further processed because of too strong motion artifacts. From the remaining seven measurements, we could extract 11 sequences which were suitable for further evaluation and to which the saturation model was applied. Nevertheless, further six sequences were excluded, because they contained less than 675 frames (corresponding to half of the 1350 frames per measurement). This decision was taken because the comparison of sequences with very different frame numbers is critical, and the stabilization of eC_{final} cannot always be reliably confirmed for very low frame numbers. Five sequences remained—one sequence for each examination and two sequences for the last examination. These numbers already highlight the high loss of data due to the measurement conditions not directly related to the tracking of the MBs. In Table I, the results of the remaining sequences are summarized. Nevertheless, an improvement of the investigator's performance is recognizable: because of few out-of-plane movements, the number of frames that could be assigned to one sequence increases for the last examinations.

To complete the information also the motion estimated in the sequences and the number of tracked MBs are given.

A. Saturation Model and Acquisition Times

Applying the saturation model and evaluating the stabilization of eC_{final} or erBV$_{\text{final}}$, we found the following criteria to be suitable for the assessment of the sequences.

1) The quality of fit should be $R^2 \ge 0.98$.
2) The percentage of the reconstruction should be $25\% \le pR \le 100\%$.
3) eC_{final} or erBV$_{\text{final}}$ should stabilize for shortened measurement times.

To illustrate the application of the saturation model and for a better comprehension of the results given in Table I, the exponential fits to the MIOT and mULM data of the second examination (highest vascularization) are depicted in Fig. 1. In Fig. 1(a), the rBV values derived from MIOT are plotted as the function of the frame number (solid line) and the exponential fit to these values is plotted with a dashed line. In Fig. 1(b), erBV$_{\text{final}}$ for shortened measurement times (stepwise by 50 frames) are visualized, showing no stabilization. Because of $pR > 100\%$, $R^2 < 0.98$, and the missing stabilization, rBV$_{\text{final}}$ should be questioned. In Fig. 1(c) and (d), the corresponding results derived from the mULM are shown. Here, eC_{final} already stabilized after 300 frames and pR and R^2 fulfil the described criteria.

However, from Table I it becomes clear, that both measurements of the last examination do not fulfil these criteria for the data based on the mULM and, therefore, they must be interpreted with care. For the MIOT results, the sequences of the first and second examinations, and the second measurement of the last examination do not fulfil these criteria.

From the pR values obtained applying the saturation model, a rough estimate of the acquisition times needed for the reconstruction of 90% of the vasculature can be derived. If a constant MB concentration during the measurement could be assumed and the measurements had not to be subdivided into sequences, the acquisition time $t_{90\%}$ that is needed would be

$$t_{90\%} = \frac{\text{frames}}{f_s} \frac{\ln(1 - 0.9)}{\ln(1 - pR)} \quad (8)$$

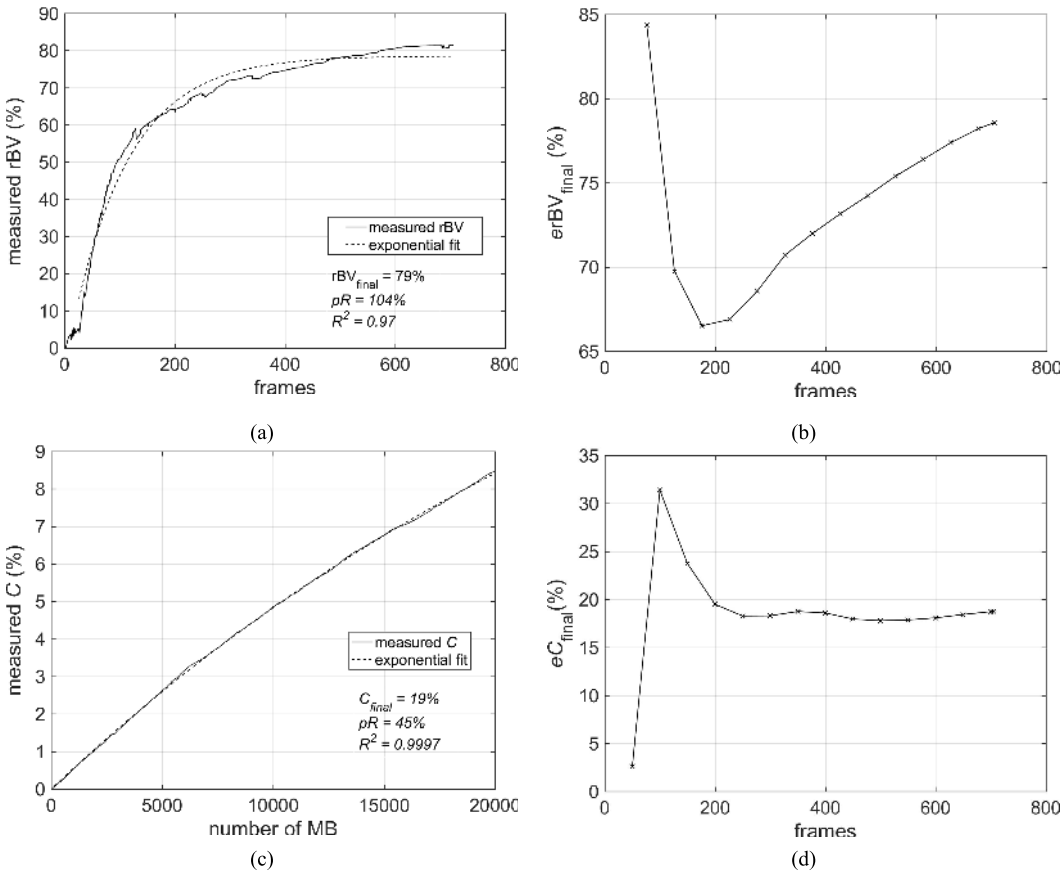

Fig. 1. Applying the saturation model to the data of the second examination (e2/m1/s5). (a) Measured rBV (solid line) derived from MIOT and exponential fit (dashed line). (b) Estimated final erBV$_{\text{final}}$ for shortened measurement times (stepwise by 50 frames). (c) Measured C (solid line) derived from mULM and exponential fit (dashed line). (d) Estimated final eC_{final} for shortened measurement times.

with the frame rate f_s. For the examinations 1–3, the estimate of $t_{90\%}$ is between 180 and 350 s.

B. Visualization

The images obtained from the second examination are exemplarily shown in Fig. 2. In Fig. 2(a), a conventional B-mode image is depicted. The tumor ROI is marked in red. In Fig. 2(b), the MIOT data are shown. In Fig. 2(c) and (d), the information derived from the mULM is visualized: the occurrence and the velocity map, respectively. In Fig. 2(e), the four zoomed-in view regions marked in Fig. 2(c) and (d) are presented showing the occurrences and the velocities and additionally the flow directions. It can be seen, that the marked tumor in the B-mode image is mainly characterized by a hypoechoic region providing no information about the vasculature. In contrast, the MIOT data totally overfill the B-mode image indicating a high rBV, but neither providing the detailed information on the vascularization. On the other hand, the occurrence and velocity maps derived from mULM give an impression of the structuring and complexity of the vessels. They better highlight the higher perfusion at the right border of the tumor. The zoomed-in view regions further highlight the high resolution that can be obtained with mULM.

C. MB Concentration and Tissue Motion

In Fig. 3, the highly varying MB concentration during the measurements is exemplarily shown by plotting the number of detections per frame (again for the second examination). At the same time, the results of the processing described in Section II-B are shown. Due to the out-of-plane movements, the measurement had to be subdivided into five sequences. Here, the frames which were assigned to sequence 4 are coded in red, the frames assigned to sequence 5 in green (sequences 1–3 are not shown, because each contained only a few frames of few detections). Searching for correlating frames within the complete measurement allowed to extract longer sequences although the frames are not necessarily connected. Finally, only the results of sequence 5 were accepted in Table I. There, also the amount of compensated in-plane motion is given for each sequence.

IV. Discussion

In contrast to preclinical measurements in anesthetized mice with induced and clearly definable tumors, an optimized injection scheme, and comparable small motions, the acquisition and processing of clinical data is more challenging. The focus of this preliminary study was to gain experience for the establishment of ULM in clinical routine.

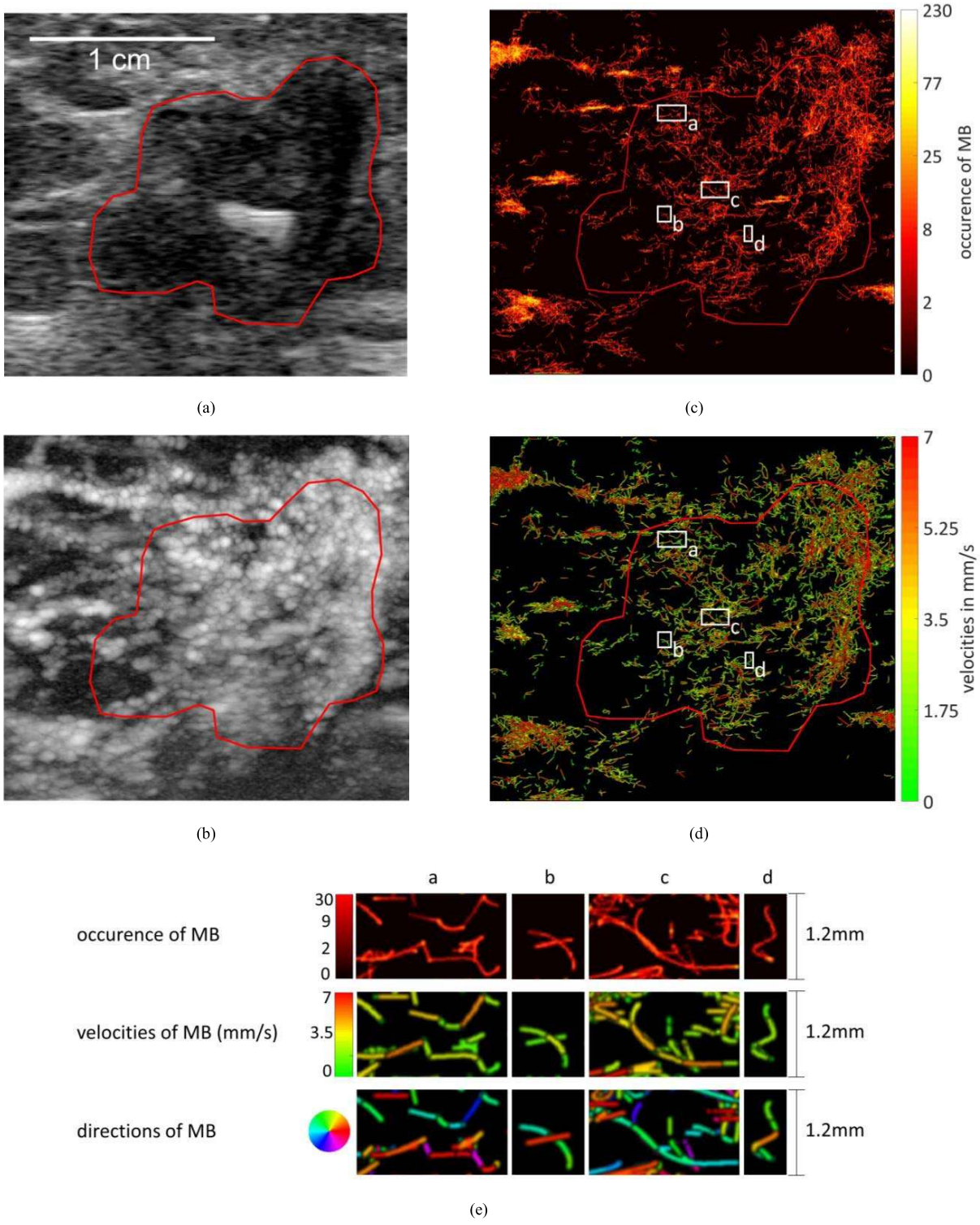

Fig. 2. (a) B-mode image with the tumor ROI marked in red. (b) Image containing the MIOT data. (c) Occurrence map and (d) velocity map derived from the mULM for the second examination (e2/m1/s5). (e) Zoomed-in view regions marked in (c) and (d) showing the occurrence of the tracked MBs (first row), the flow velocities and directions (second and third rows, respectively).

It is shown that super-resolution US imaging based on the tracking of MBs provides information and visualizations beyond the established CEUS techniques (see Fig. 2). The maps derived from the tracking information are rich of details and give an impression of the complexity of the microvasculature. They further provide information about blood flow velocities—and could also provide information about the flow directions (not shown)—and allow to differentiate between the smaller single capillaries and larger vessels. In comparison, the MIOT images only show a rough estimate

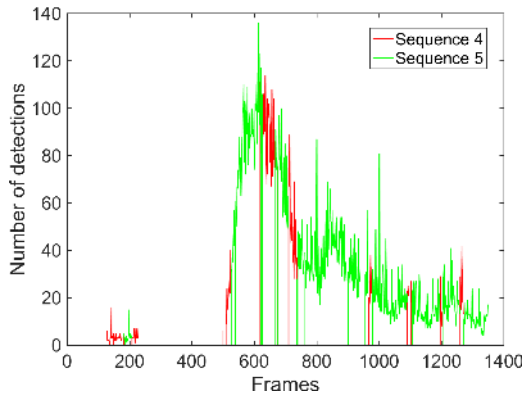

Fig. 3. Number of detections per frame during the second examination (e2/m1). Frames assigned to sequences 4 and 5 are marked in red and green, respectively. Frames assigned to sequences 1–3, and their corresponding detections are not shown.

of the degree of vascularization, whereas the blood supply cannot be assessed in the standard B-mode images.

A. Image Acquisition and Tracking of the MBs

Although, the MBs were clearly visible in the B-mode images of the preclinical measurements, in the clinical setup with its lower frequency the contrast mode had to be used for the visualization of the MBs. On the one hand, the MBs can be more easily detected in the contrast mode images and the motion estimation in the B-mode images is not disturbed by the moving MBs. Thus, considerations regarding the right order of detection, separation of MBs from tissue background and motion compensation do not apply. Finally, the detected MB positions can be easily corrected with the estimated motion. On the other hand, the use of the contrast mode in most systems leads to lower frame rates with a higher uncertainty on the actual MB tracks. However, developing adapted imaging schemes the frame rates could be increased with the MBs still clearly observable in the images.

In addition, the tracking is more challenging because of the larger slice thickness of the imaging plane leading to more overlays of vessels. In [14], we already pointed out that in the case of complex morphologies of vessel trees and for nonoptimal measurement conditions the nearest neighbor tracking is more prone to errors and, therefore, the probabilistic approach should be preferred. The results of the implemented MCMCDA are promising; however, this algorithm would also benefit from higher frame rates. Furthermore, other probabilistic approaches [21] might perform faster. Generally, the highly varying velocities of capillaries versus arterioles and venules or due to the change of in-plane to perpendicular flow are difficult to handle with linear motion models assuming constant velocity.

The overall computation time is composed of several processing steps. Dividing the sequences into subsequences took about 2 min, the motion estimation about 15 min, and the MB detection about 5 min. With regard to the tracking, the computation time strongly depends on the number of detections per frame: for 15 MB per frame it took about 0.4 s per frame, for 60 MBs about 6 s, and for 150 MBs about 35 s. Though, these processing steps were carried out separately and were not optimized regarding the processing times. Thus, the computation time should and could be reduced (e.g., with parallel computing).

B. Tissue Motion

Other difficulties arise from tissue motion. The stronger and nonrigid movements need more general deformation models and advanced motion estimation techniques in the B-mode frames which often additionally have poor tissue contrast within the tumors. Therefore, it was necessary to apply an affine image registration as proposed by Rueckert *et al.* [16] (see Section II-B). This method worked well for the correction of in-plane-movements, although it would probably also benefit from higher frame rates. Even more difficult to handle were the strong out-of-plane movements which led to a reduction of usable measurement sequences. With the procedure described in Section II-B as many long sequences as possible were gained. Nevertheless, also with the experience of the clinical investigators, the out-of-plane movement was reduced (longer sequences in the last examinations, see Table I).

C. Saturation Model

To gain information of the vasculature and estimates on the necessary improvements, we applied the saturation model we proposed in [20]. It is motivated by the fact that in clinical applications, the full vasculature often may not be reconstructed due to the short measurement times. The amount of filling of the vasculature necessary to derive clinically relevant parameters of the morphology will be of interest for future studies.

Applying the saturation model, the final rBV can be estimated, information on the percentage of reconstruction is gained, and the acquisition times needed for a stable prediction can be assessed. This way, also objective criteria can be derived about the suitability of measurements. For example, if only few MBs are detected, this can be due to a very low MB concentration or due to a minor vascularization. However, if the rBV-value saturates, this is an indication for a minor vascularization (see Table I).

D. Frame Rate, MB Concentration, and Acquisition Times

As already mentioned earlier, higher frame rates can improve the motion correction and the tracking; however, they will not have an impact on the acquisition times necessary for the full reconstruction. The total number of detected vessels within the acquisition time is influenced by the flow-rate of MBs in the vessels which depends on the blood flow in the vessels, mainly capillaries, and on the MB concentration in the blood.

Here, it became apparent that the injection protocol, i.e., injection speed and MB concentration, needs to be improved. The highly varying MB concentrations (see Fig. 3) led to a reduction of meaningful sequences. Furthermore, an overall higher MB concentration would decrease the relatively long acquisition times estimated for the reconstruction of 90% of

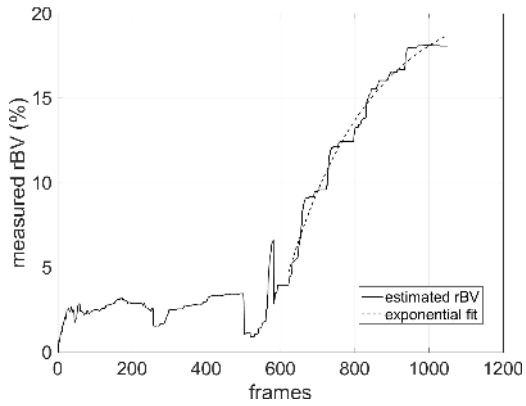

Fig. 4. Measured rBV (solid line) derived from MIOT and exponential fit (dashed line) for the last examination (e4/m1/s1). The suitable segment must be chosen interactively.

the vasculature. From the saturation model, it can be derived that, e.g., a doubled dose leads to half of the acquisition time needed. From our observations of relatively few overlapping MB signals, we assume that a higher dose rate than 0.5 mL of SonoVue up to the maximum recommended dose of 2.4 mL should be manageable. This will be further supported by novel approaches for the MB separation (e.g., van Sloun *et al.* [22]).

To jointly advance the clinical application of super-resolution US imaging, the reporting on the injection scheme, on the number of detected and tracked MBs, and on the measurement times should be standardized.

E. Comparison to MIOT

Although the established CEUS technique MIOT is stated to be robust [10], its analysis also suffers from the in-plane and out-of-plane movements. Furthermore, the truncation of sequences and the varying MB concentrations impede techniques like the calculation of replenishment kinetics or perfusion parameters, e.g., see [23]. In the case of the mULM data, the use of the saturation model compensates for a varying MB concentration during the measurement. (The independent variable of the exponential model is the number of detected MBs.) In the case of the MIOT data, this is not possible (the independent variable is the frame number/acquisition time), so usable segments must be chosen interactively (see Fig. 4) or even might not be available.

F. Pixel Size

We decided to set the pixel size of the visualizations to 10 μm because of practical assumptions. The theoretical limit of the localization accuracy given by Desailly *et al.* [24] would be below 1 μm (rough estimation based on the limited information provided by Canon). Viessmann *et al.* [25] proved a localization precision of 4.7 and 2 μm in the lateral and axial directions, respectively, in an *in vitro* setup with a comparable US system (Toshiba Aplio XG, PVT382BT). Measurements of the actual resolution without ground truth are difficult because estimating the resolution based on lateral profiles of small vessels [4], [15] is only applicable if a certain number of MBs passed through the vessel. Only if two clear flow profiles are recognizable the existence of two vessels can be assumed, otherwise single tracks could belong to one larger vessel. These profiles are typically available for larger vessels which—on the other hand—might not provide the lower bound of accuracy.

However, since the MB detection is limited by the chosen resolution of 5 μm (see Section II-C), a pixel size of 10 μm seems to be reasonable for the super-resolution visualizations. This is substantially lower than the pixel size of 71 μm (lateral and axial) of the US device. Furthermore, the diameter of capillaries is typically between 5 and 10 μm. Thus, for the estimation of the rBV, it is reasonable to model one track with an equivalent thickness. Finally, the capillaries might not be visible in the visualization if drawn thinner.

G. Clinical Interest

Super-resolution imaging can bridge the gap between the histological—and thus invasive—analysis of tumors and the poor resolution of the current noninvasive imaging techniques. The monitoring of antiangiogenic cancer therapy is already feasible with MIOT [11], but the more detailed morphological and the functional information (e.g., flow velocities) of super-resolution imaging could provide new insights into the angiogenesis of tumors and give essential information for the improvement of the therapeutic benefit. Besides, a radiomic analysis of various quantitative parameters that comprise very different morphological and functional aspects of the vasculature could enable the automated discrimination of different tumor types.

Moreover, super-resolution US imaging may not only be applied in oncology but could also be of interest for a multitude of other applications, e.g., for the characterization of inflamed tissues, risk assessment of atherosclerosis by imaging the vasa vasorum, the identification of immunological disorders or organ fibrosis, the monitoring of the revascularization in ischemic tissues, or the differentiation of benign and malign nevi.

H. Perspectives

Advancing super-resolution US imaging to 3-D, some of the mentioned challenges could be overcome. For example, out-of-plane motion and slice thickness would become irrelevant. Furthermore, with 2-D imaging only the in-plane flow velocities can be determined. In contrast, the 3-D techniques will allow the correct determination of the flow velocities and directions and the reconstruction of vessel trees also for complex morphologies. In addition, the relocalization of the imaged ROI for monitoring would be easier. We believe that the prevalence of devices equipped with 2-D matrix transducers will increase as soon as their benefit in clinical routine is proven.

V. Conclusion

We could show that clinical super-resolution imaging is feasible with a single contrast agent injection within measurement times of less than 5 min. Although vessel trees were not imaged completely with the statistical sampling by the MBs,

relevant parameters could be derived also from incomplete vessel trees by investigating their reconstruction over time. In addition, the amount of coverage and the final coverage could be estimated and allowed to assess the quality of the vascular image.

ACKNOWLEDGMENT

The authors acknowledge the contribution of A. Rix to the clinical measurements.

REFERENCES

[1] O. Couture, B. Besson, G. Montaldo, M. Fink, and M. Tanter, "Microbubble ultrasound super-localization imaging (MUSLI)," in *Proc. IEEE IUS*, Oct. 2011, pp. 1285–1287.
[2] M. Siepmann, G. Schmitz, J. Bzyl, M. Palmowski, and F. Kiessling, "Imaging tumor vascularity by tracing single microbubbles," in *Proc. IEEE IUS*, Oct. 2011, pp. 1906–1909.
[3] K. Christensen-Jeffries, R. J. Browning, M.-X. Tang, C. Dunsby, and R. J. Eckersley, "*In vivo* acoustic super-resolution and super-resolved velocity mapping using microbubbles," *IEEE Trans. Med. Imag.*, vol. 34, no. 2, pp. 433–440, Feb. 2015.
[4] C. Errico *et al.*, "Ultrafast ultrasound localization microscopy for deep super-resolution vascular imaging," *Nature*, vol. 527, no. 7579, pp. 499–502, Nov. 2015.
[5] D. Ackermann, G. Schmitz, and S. Member, "Detection and tracking of multiple microbubbles in ultrasound B-mode images," *IEEE Trans. Ultrason., Ferroelectr., Freq. Control*, vol. 63, no. 1, pp. 72–82, Jan. 2016.
[6] P. Carmeliet and R. K. Jain, "Molecular mechanisms and clinical applications of angiogenesis," *Nature*, vol. 473, pp. 298–307, May 2011.
[7] E. Ruoslahti, "Specialization of tumour vasculature," *Nature Rev. Cancer*, vol. 2, pp. 83–90, Feb. 2002.
[8] J. Ehling *et al.*, "Micro-CT imaging of tumor angiogenesis: Quantitative measures describing micromorphology and vascularization," *Amer. J. Pathol.*, vol. 184, pp. 431–441, Feb. 2014.
[9] C. M. Park *et al.*, "Fn13762 murine breast cancer: Region-by-region correlation of first-pass perfusion CT indexes with histologic vascular parameters," *Radiology*, vol. 251, no. 3, pp. 721–730, 2009.
[10] M. Palmowski *et al.*, "Comparison of conventional time–intensity curves vs. Maximum intensity over time for post-processing of dynamic contrast-enhanced ultrasound," *Eur. J. Radiol.*, vol. 75, no. 1, pp. e149–e153, 2010.
[11] M. A. Pysz, K. Foygel, C. M. Panje, A. Needles, L. Tian, and J. K. Willmann, "Assessment and monitoring tumor vascularity with contrast-enhanced ultrasound maximum intensity persistence imaging," *Invest. Radiol.*, vol. 46, no. 3, pp. 187–195, Mar. 2011.
[12] K. Wei, A. R. Jayaweera, S. Firoozan, A. Linka, D. M. Skyba, and S. Kaul, "Quantification of myocardial blood flow with ultrasound-induced destruction of microbubbles administered as a constant venous infusion," *Circulation*, vol. 97, pp. 473–483, Feb. 1998.
[13] B. Theek, T. Opacic, D. Möckel, G. Schmitz, T. Lammers, and F. Kiessling, "Automated generation of reliable blood velocity parameter maps from contrast-enhanced ultrasound data," *Contrast Media Mol. Imag.*, vol. 2017, May 2017, Art. no. 2098324.
[14] S. Dencks, D. Ackermann, and G. Schmitz, "Evaluation of bubble tracking algorithms for super-resolution imaging of microvessels," in *Proc. IEEE IUS*, Sep. 2016, pp. 1–4.
[15] T. Opacic *et al.*, "Motion model ultrasound localization microscopy for preclinical and clinical multiparametric tumor characterization," *Nature Commun.*, vol. 9, Apr. 2018, Art. no. 1527.
[16] D. Rueckert, L. I. Sonoda, C. Hayes, D. L. G. Hill, M. O. Leach, and D. J. Hawkes, "Nonrigid registration using free-form deformations: Application to breast MR images," *IEEE Trans. Med. Imag.*, vol. 18, no. 8, pp. 712–721, Aug. 1999.
[17] D.-J. Kroon. (2011). *B-Spline Grid, Image and Point Based Registration*. [Online]. Available: https://de.mathworks.com/matlabcentral/fileexchange/20057-b-spline-grid–image-and-point-based-registration
[18] S. Oh, S. Russell, and S. Sastry, "Markov chain Monte Carlo data association for multi-target tracking," *IEEE Trans. Autom. Control*, vol. 54, no. 3, pp. 481–497, Mar. 2009.
[19] R. C. Gessner, C. B. Frederick, F. S. Foster, and P. A. Dayton, "Acoustic angiography: A new imaging modality for assessing microvasculature architecture," *Int. J. Biomed. Imag.*, vol. 2013, Jun. 2013, Art. no. 936593.
[20] S. Dencks, M. Piepenbrock, G. Schmitz, T. Opacic, and F. Kiessling, "Determination of adequate measurement times for super-resolution characterization of tumor vascularization," in *Proc. IEEE IUS*, Sep. 2017, pp. 1–4.
[21] P. Song *et al.*, "Improved super-resolution ultrasound microvessel imaging with spatiotemporal nonlocal means filtering and bipartite graph-based microbubble tracking," *IEEE Trans. Ultrason., Ferroelectr., Freq. Control*, vol. 65, no. 2, pp. 149–167, Feb. 2018.
[22] R. J. G. van Sloun, O. Solomon, Y. C. Eldar, H. Wijkstra, and M. Mischi, "Sparsity-driven super-resolution in clinical contrast-enhanced ultrasound," in *Proc. IEEE IUS*, Sep. 2017, pp. 1–4.
[23] M. Krix, F. Kiessling, N. Farhan, K. Schmidt, J. Hoffend, and S. Delorme, "A multivessel model describing replenishment kinetics of ultrasound contrast agent for quantification of tissue perfusion," *Ultrasound Med. Biol.*, vol. 29, pp. 1421–1430, Oct. 2003.
[24] Y. Desailly, J. Pierre, O. Couture, and M. Tanter, "Resolution limits of ultrafast ultrasound localization microscopy," *Phys. Med. Biol.*, vol. 60, no. 22, pp. 8723–8740, 2015.
[25] O. M. Viessmann, R. J. Eckersley, K. Christensen-Jeffries, M. X. Tang, and C. Dunsby, "Acoustic super-resolution with ultrasound and microbubbles," *Phys. Med. Biol.*, vol. 58, no. 18, p. 6447, Sep. 2013.

Stefanie Dencks (M'12) studied electrical engineering at the University of Hanover, Hanover, Germany, and continued her studies of biomedical engineering at the Technical University of Dresden, Dresden, Germany, where she received the Dipl.-Ing. degree in 2002. She received the Dr.-Ing. degree in electrical engineering from Ruhr University Bochum, Bochum, Germany, in 2009.

In 2003, she joined the Medical Physics Group, Diagnostic Radiology Department, University Hospital, Kiel, Germany, where she focused on ultrasound characterization of bone and ultrasonic signal analysis in cooperation with Ruhr University Bochum. From 2009 to 2011, she was a Research Staff Member with the Ultrasound Department, Physikalisch-Technische Bundesanstalt, Brunswick, Germany, where she did research on monitoring high-intensity focused ultrasound therapy. Since 2011, she has been a Senior Scientist with the Chair of Medical Engineering, Ruhr University Bochum. Her general research interests are signal analysis and image processing for medical ultrasound, with current applications in super-resolution imaging with contrast agents and the enhancement of cannula visibility in medical interventions.

Marion Piepenbrock studied medical physics at TU Dortmund, Dortmund, Germany, and received the B.Sc. and M.Sc. degrees in 2014 and 2016, respectively. She is currently pursuing the Ph.D. degree in electrical engineering at the Chair for Medical Engineering, Ruhr University Bochum, Bochum, Germany.

Her research interests focus on image processing of medical ultrasound, especially super-resolution imaging with ultrasound contrast agents.

Tatjana Opacic, photograph and biography not available at the time of publication.

Barbara Krauspe, photograph and biography not available at the time of publication.

Elmar Stickeler, photograph and biography not available at the time of publication.

Fabian Kiessling was born in Mannheim, Germany, in 1972. He studied medicine at the University of Heidelberg, Heidelberg, Germany.

He performed his clinical training with the German Cancer Research Center (DKFZ), and with different clinical departments of the University of Heidelberg. In 2003, he was appointed as the Leader of a Molecular Imaging Group, Department of Medical Physics in Radiology, DKFZ. In 2008, he became a member of the Directorate of the Helmholtz Institute for Biomedical Engineering and was appointed as the Director of the Institute for Experimental Molecular Imaging, RWTH Aachen University, Aachen, Germany. He has authored over 300 scientific publications and book chapters and edited three books.

Dr. Kiessling received the Emil Salzer Prize for Cancer Research and the Richtzenhain Prize. He serves on the Editorial Board for several scientific journals including *Radiology*, *European Radiology*, *European Radiology Experimental*, *American Journal of Nuclear Medicine and Molecular Imaging*, and *Nanotheranostics*. He is currently Treasurer of the European Society for Molecular Imaging (ESMI), a Founding Member of the ESMI working group Image-Guided Drug Delivery, and he was Chairman of the "Molecular Imaging" subcommittee of the European Society for Radiology. Furthermore, he was the Program Chair of the World Molecular Imaging Conference in New York, NY, USA, in 2016.

Georg Schmitz (S'89–M'98–SM'05) was born in Mülheim an der Ruhr, Germany, in 1965. He received the Dipl.-Ing. and Dr.-Ing. degrees in electrical engineering from Ruhr University Bochum, Bochum, Germany, 1990 and 1995, respectively.

From 1995 to 2001, he was a Principal Scientist with the Philips Research Laboratories of Royal Philips Electronics, Hamburg and Aachen, Germany. From 2001 to 2004, he was a Professor of medical engineering with the University of Applied Science Koblenz, Koblenz, Germany. Since 2004, he has been a Professor of electrical engineering and the Chair of Medical Engineering with Ruhr University Bochum. His research interests are in the field of ultrasonic imaging and signal processing with current research projects on nonlinear image reconstruction, photoacoustic imaging, and super-resolution imaging using ultrasound localization microscopy.

Dr. Schmitz is a member of the Acoustical Society of America, the German Association of Electrical Engineers (VDE), World, European and German Societies of Ultrasound in Medicine and Biology (WFUMB, EFSUMB, DEGUM), and Editorial Advisory Board of Ultrasound in Medicine and Biology. He serves as an Associate Editor for IEEE TRANSACTIONS ON ULTRASONICS, FERROELECTRICS, AND FREQUENCY CONTROL.